American Mineralogist, Volume 80, pages 680–690, 1995

Tetrahedral rigid-body motion in silicates

K. L. Bartelmehs
Department of Geological Sciences, University of Texas at Austin, Austin, Texas 78712, U.S.A.

R. T. Downs
Carnegie Institution of Washington, 5251 Broad Branch Road NW, Washington, DC 20015, U.S.A.

G. V. Gibbs
Department of Materials Science and Engineering and Department of Geological Sciences, Virginia Polytechnic Institute and State University, Blacksburg, Virginia 24061, U.S.A.

M. B. Boisen, Jr.
Department of Mathematics, Virginia Polytechnic Institute and State University, Blacksburg, Virginia 24061, U.S.A.

J. B. Birch
Department of Statistics, Virginia Polytechnic Institute and State University, Blacksburg, Virginia 24061, U.S.A.

Abstract

The atomic displacement parameters (ADPs) obtained from published refinements of silicate crystals measured at or below room temperature are examined to determine if TO_4 (T = Al,Si) tetrahedra display rigid-body thermal motion. In many cases, the correlation found among the ADPs is consistent with the **TLS** model of rigid-body motion. For these data, the translational motion is described by the ADPs of the central T atom, whereas both librational and translational motion are displayed in those of the surrounding O atoms. The libration angle for rigid tetrahedra is quadratically dependent on the difference between the isotropic equivalent displacement parameter of the T and O atoms, $B_{eq}(T)$ and $B_{eq}(O)$, respectively. The value of $B_{eq}(O)$ is on average twice that of $B_{eq}(T)$, with an observed maximum value of ~2.0 Å^2. Variation in the observed Si-O bond lengths of rigid tetrahedra in the silica polymorphs is related only to the fractional s-character of O, $f_s(O)$. ADPs that do not indicate rigid-body motion for a given tetrahedron may be used to identify crystals containing disorder or suggest problems with the refinement.

Introduction

For our purposes, a rigid body consists of a group of atoms that maintain constant interatomic separations regardless of any displacement of its atoms. Therefore, rigid-body motion requires that the motions of all the individual atoms of the group be correlated (Johnson, 1970). The terms "rather rigid" and "quasi-rigid" have been used to describe the vibrational motion of SiO_4 tetrahedra in quartz (Liebau and Böhm, 1982), and various models have assumed rigid tetrahedra to describe the α-β phase transition (Megaw, 1973; Boysen et al., 1980; Liebau and Böhm, 1982; Ghose et al., 1986). Grimm and Dorner (1975) used a bonding model based on sp^3 σ-orbitals to infer that the tetrahedra in quartz are rigid. Rigid tetrahedra have also been assumed in lattice dynamical calculations (for instance, Rao et al., 1988) and bond-length corrections (Ghose et al., 1986; Downs et al., 1992). Computer models for silica have been constructed assuming rigid tetrahedra (Stixrude and Bukowinski, 1988). Here, we examine the vibrational motion measured by X-ray diffraction for experimental evidence to support the assertion of TO_4 rigid-body motion.

Atomic displacement parameters (ADPs), routinely used as regressor variables in a refinement model to describe the time-and-space-averaged displacements of an atom from its mean position, have provided important physical information about crystals. Several studies have focused on the difference displacement parameter, Δ_{AB}, evaluated along the vector between two adjacent atoms, A and B, where

$$\begin{aligned}\Delta_{AB} &= z^2_{BA} - z^2_{AB} \\ &= [\mathbf{v}]^t_{D^*}[D(U_B - U_A)D][\mathbf{v}]_{D^*} \\ &= \frac{1}{2\pi^2}[\mathbf{v}]^t_{D^*}(\beta_B - \beta_A)[\mathbf{v}]_{D^*}\end{aligned}$$

and z^2_{BA} and z^2_{AB} are the respective mean-square-displacement amplitudes (MSDAs) of B toward A and of A toward B, $[\mathbf{v}]_{D^*}$ is a unit vector parallel to the AB direction defined in terms of the reciprocal basis $D^* = \{\mathbf{a}^*,\mathbf{b}^*,\mathbf{c}^*\}$,

0003–004X/95/0708–0680$02.00

β_A (or U_A) and β_B (or U_B) are the ADP matrices (or temperature-factor matrices) for A and B, respectively; and D is a diagonal matrix containing the magnitudes of **a***, **b***, and **c***. Not only can Δ_{AB} provide a measure of relative internal motion between atoms A and B (Dunitz et al., 1988), but it also provides a measure of the spin state for transition metals (Chandrasekhar and Bürgi, 1984) and the Jahn-Teller deformation of Cu complexes (Bürgi, 1984), and it has been used to detect errors in structure refinement models and in published results (Hirshfeld, 1976; Trueblood, 1978; Dunitz et al., 1988; Kunz and Armbruster, 1990). In framework silicate and aluminosilicate crystals, the average of the four Δ_{TO} values for a given tetrahedron, $\langle\Delta_{TO}\rangle$, provides a measure of positional and structural disorder (Kunz and Armbruster, 1988, 1990; Downs et al., 1990). Large values of Δ_{XO} recorded for pyrope (X = Mg), almandine (X = Fe), and andradite (X = Ca) have been taken as evidence for positional disorder or rattling-type motion of the X atom (Armbruster and Geiger, 1993). Downs et al. (1990) also found that the average vibrational motion between the T and O atoms in framework silicates is consistent with a rigid T-O bond.

As a test of the assertion that TO_4 tetrahedra behave as rigid bodies, the ADPs of the T and O atoms in TO_4 groups obtained from refinements of silicate structures are examined for experimental evidence consistent with rigid-body vibrational motion. This is accomplished by measuring the agreement between the observed ADPs and those calculated using the **TLS** model of rigid-body motion (Schomaker and Trueblood, 1968). The tetrahedral groups are examined for correlated motion represented in the sizes, shapes, and orientations displayed by the ADPs of the atoms in the group. The analysis is completed by examining the applicability of the rigid-body hypotheses to the ADP data and the constraints placed on the data by rigid-body motion.

Data selection and evidence of rigid T-O bonds in nonframework silicates

In an examination of the relationship between z^2_{OT} and z^2_{TO} in framework silicate crystals, Downs et al. (1990) found that the ADPs determined for crystals free of static disorder are consistent with rigid T-O bond vibrational motion. If the forces that govern the geometry of TO_4 tetrahedra are short ranged (Gibbs, 1982), then the T and O atoms of tetrahedra in all silicate structures should exhibit similar vibrational motion. Therefore, the Δ_{TO} values determined for nonframework silicates should represent vibrational motion consistent with that found for ordered framework silicates. For such structures, Downs et al. (1990) proposed criteria to identify rigid T-O bond behavior on the basis of the distributional properties of $\langle\langle\Delta_{TO}\rangle\rangle$, the average of all the $\langle\Delta_{TO}\rangle$ values in a structure. On the basis of these criteria, they concluded that about one-third of the structures examined display rigid T-O bonds. However, about 130 of the 670 individual Δ_{TO} values in their study exceed their allowed maximum deviation from zero (± 0.0015 Å^2). Therefore, in this study more restrictive criteria are used that are based on the $\langle\Delta_{TO}\rangle$ values rather than values from the ensemble of tetrahedra. The revised criteria are (1) -0.00125 Å$^2 \leq \langle\Delta_{TO}\rangle \leq 0.002$ Å^2 and (2) the estimated standard deviation of $\langle\Delta_{TO}\rangle \leq 0.00125$ Å^2. Nonframework tetrahedra that satisfy these criteria would provide evidence of rigid T-O bond vibrational motion similar to that found in framework silicates. These criteria also provide a measure of both the relative perfection of the crystal and the physical acceptability of the results provided by the refinement (Hirshfeld, 1976; Dunitz et al., 1988; Kunz and Armbruster, 1990; Downs et al., 1990).

The criteria were first applied to 469 silicate tetrahedra obtained from refinements of framework structures with diffraction data collected at standard conditions (Downs et al., 1990). The analysis indicates that 35% (166) of the 469 tetrahedra satisfy both criteria and qualify as displaying rigid T-O bonds. Of the 357 tetrahedra in nonframework structures obtained for this study (Appendix 1), 50% (186) satisfy both criteria. Thus, there is additional evidence provided by the ADPs from nonframework silicates to support the assertion that the T-O bond vibrates like a rigid rod (Downs et al., 1990). The relatively low percentages of framework and sheet silicate tetrahedra that satisfy (1) and (2) [35 and 12%, respectively, vs. 50–68% for ortho-, soro-, chain, and ring silicates (Appendix 1)] suggest that substitutional and structural disorder is more common in these structure types. Collectively, the ADPs for 352 tetrahedra that satisfy both criteria appear to represent groups either from crystals without static disorder or twinning or from refinements that correctly modeled these effects, along with correctly reported ADPs, and thus provide a good data set for the study of the vibrational motion of TO_4 tetrahedra (Hirshfeld, 1976).

Rigid-body analysis

In our examination of the average vibrational motion of TO_4 tetrahedra, the observed ADPs for each T and O atom were compared with those calculated using the **TLS** model of rigid-body motion (Schomaker and Trueblood, 1968). On the one hand, it has been asserted by Hummel et al. (1990) and Chandrasekhar and Bürgi (1984), for example, that coordination polyhedra behave as rigid bodies if a model based on rigid motion reproduces the experimental ADPs observed for the polyhedra to within experimental error. In fact, several methods based on differences between observed and calculated ADPs have been proposed to measure how well such calculations reproduce a set of observed ADPs (Burns et al., 1967; Destro et al., 1977; Trueblood, 1978; Hummel et al., 1990). On the other hand, as the **TLS** parameters obtained in a least-squares refinement can incorporate the effects of internal motions of the individual atoms, Dunitz et al. (1988) have argued that such agreement does not necessarily

mean that a coordinated polyhedron or a molecule behaves as a rigid body.

The agreement between observed and calculated ADPs was evaluated in this study using a strategy based on that devised by Burns et al. (1967). In their strategy, three parameters (here referred to as ellipsoid agreement parameters, EAPs) were defined that measure the agreement in size, shape, and orientation between the calculated and observed thermal ellipsoids of an atom. For this study, if the three EAPs for each of the five atoms of the TO_4 tetrahedron satisfy the established agreement criteria (Appendix 2), then the thermal motion represented by the observed ADPs of the TO_4 tetrahedron is considered to be consistent with that predicted by rigid-body motion.

Such motion implies that the vibrational behavior of all atoms in the group is highly correlated (Johnson, 1970; Ghose et al., 1986). However, the assumption made in most crystal structure refinement models is that the atomic coordinates of nonequivalent atoms and their ADPs are independent and uncorrelated (the IAM model). Notwithstanding this assumption, if a group of atoms is actually rigid, then the required correlated motion should manifest itself through the relative sizes, shapes, and orientations of the refined thermal ellipsoids. By applying the EAP criteria, an observed set of ADPs can be examined for correlated motion by comparing their physical aspects (size, shape, and orientation) with the set of calculated ADPs. The EAP method chosen here is believed to be a more robust measure of fit than that involving the absolute values of observed ADPs, which can absorb systematic errors in the diffraction data (Chandrasekhar and Bürgi, 1984; Bürgi, 1984; Dunitz et al., 1988; Armbruster et al., 1990). Furthermore, this method does not rely on statistical information, which frequently is either not provided or inaccurately provided with published refinements (Trueblood, 1978; Dunitz et al., 1988). The EAP method is similar in principle to the visual methods used by Hummel et al. (1990) to study discrepancies between observed ADPs and those predicted by various models.

Each of 352 sets of observed ADPs was regressed against the 20 parameters required to define a general **TLS** model of rigid-body motion (Schomaker and Trueblood, 1968), using the program **TLS** and assuming C_1 point symmetry (Downs et al., 1992). Final parameter estimates were computed relative to the center of reaction (Schomaker and Trueblood, 1968; Johnson, 1970). Partial t tests computed for estimates of S_{ij} usually indicated a lack of statistical significance. As a result, we do not discuss the properties of the **S** matrix. Nonpositive definite **T** or **L** matrices were obtained for 39 tetrahedra. As these represent physically unrealistic results, only the remaining 313 tetrahedra were used for further analysis.

To appreciate the agreement between the observed and calculated ADPs as they relate to the EAP criteria, drawings were made of the observed and calculated thermal ellipsoids of several TO_4 groups. For example, Figure 1 compares a set of thermal ellipsoids of two tetrahedra taken from a refinement of triclinic bikitaite (Bissert and Liebau, 1986). The agreement between the size, shape, and orientation of the observed and calculated thermal ellipsoids of the T4 tetrahedron (Fig. 1a) that passes the criteria is strikingly good. However, the drawings for the Al5 tetrahedron, which fails the criteria, show distinct differences between the observed and calculated thermal ellipsoids of some of the atoms (Fig. 1b). Since the tetrahedron in Figure 1a passes our EAP criteria, the observed set of ADPs for the T4 tetrahedron is concluded to represent correlated motion that is consistent with that predicted assuming rigid-body motion. The EAP criteria calculated for the ADPs displayed in Figure 1b indicate unsatisfactory agreement between shape and orientation for three atoms of the Al5 tetrahedron. Hence, we conclude that the ADPs of the Al5 tetrahedron do not completely represent correlated thermal motion and therefore are not consistent with rigid-body motion. This does not mean that the Al5 tetrahedron is not rigid but only that the ADP data do not show it.

Application of the EAP criteria indicates that the ADPs of 105 tetrahedra are consistent with rigid-body motion of a TO_4 group. There are several reasons why two-thirds of the tetrahedra fail the EAP criteria: (1) strict application of the criteria, such that if the ADPs of only a single atom fail the criteria, the tetrahedron was rejected; (2) typographical errors in the reported data; (3) O or T atom positional disorder; (4) problems in the refinement of the ADPs, such as systematic errors caused by inadequate correction for extinction, absorption, etc.; and (5) nonrigid tetrahedra. Because a significant number of tetrahedra from all silicate structure types pass the criteria, we conclude that there is sufficient experimental evidence to support the assertion of TO_4 rigid-body motion in silicates.

Systematics of rigid tetrahedra

The 105 tetrahedra that pass the EAP criteria are listed in Table 1. Note that the table includes the SiO_4 data of enstatite used in the rigid-body analysis by Ghose et al. (1986). This is the only other silicate in this data set for which an analysis has been completed. The table also includes the estimated libration angle θ, ($\theta = \sqrt{L_{11} + L_{22} + L_{33}} \cdot 180°/\pi$) calculated from the trace of the **L** matrix determined for each tetrahedron. The θ range for all these tetrahedra (2–7°) is in good agreement with the 6–9° upper limit for the applicability of the **TLS** model suggested by Trueblood (1978).

The mean libration angle, $\langle\theta\rangle$, of the seven lowest temperature (<20 K) data ($\langle\theta\rangle$ = 3.0°) is significantly smaller than the mean libration angle of the 94 room-temperature data ($\langle\theta\rangle$ = 4.4°), indicating that the librational motion of a rigid TO_4 tetrahedron tends to increase, as expected, with temperature (Armbruster and Geiger, 1993). Indeed, for the low albite and microcline data listed in Table 1, Figure 2 shows that the libration angle increases regularly with the temperature at which the data set was recorded. For the 13 olivine structures determined at room temperature, $\langle\theta\rangle$ = 3.1°, which is similar to the mean low-

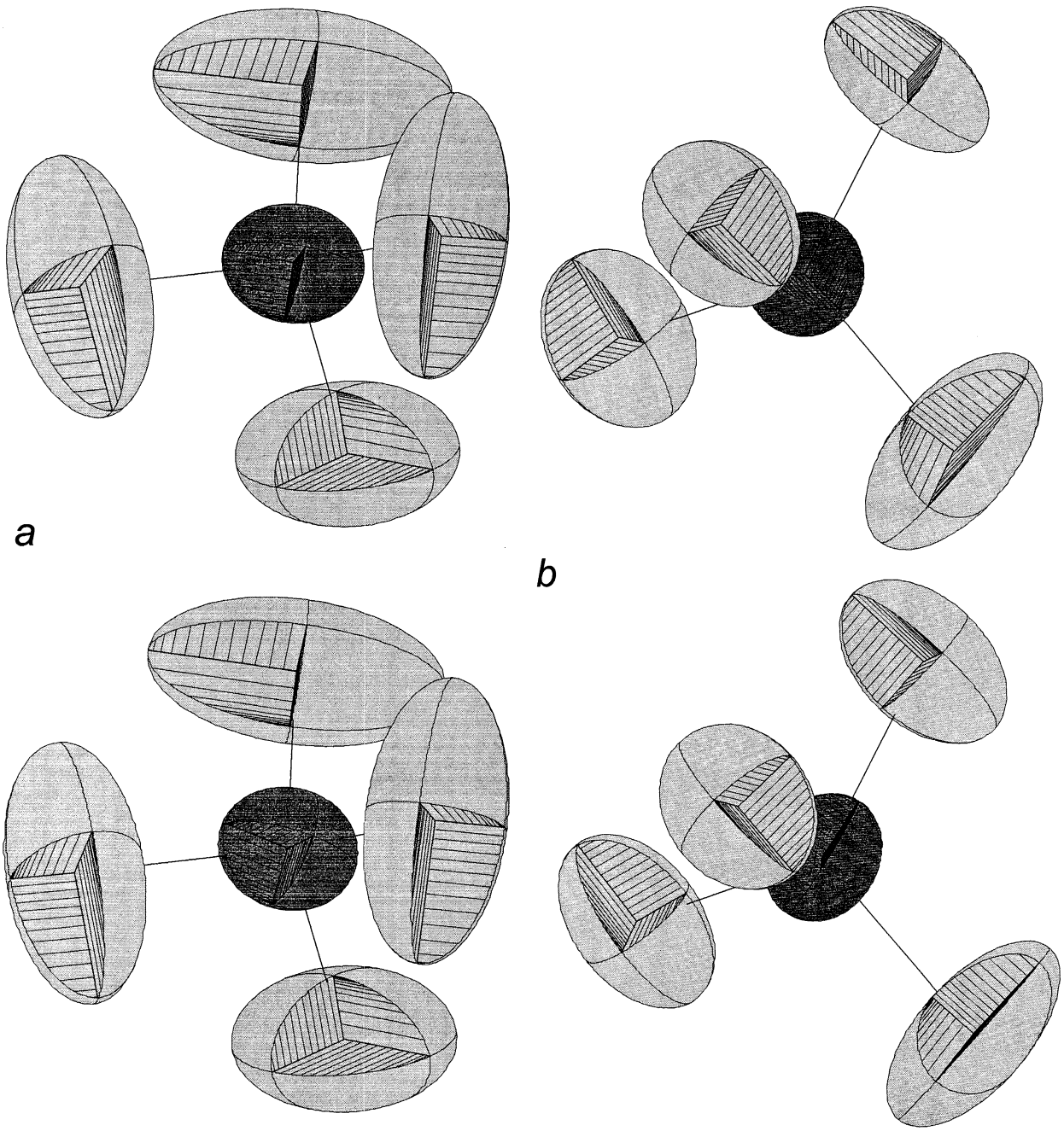

Fig. 1. (**a**) A comparison of the observed thermal ellipsoids of the T4 tetrahedron taken from a refinement of triclinic bikitaite (top) (Bissert and Liebau, 1986) vs. those calculated using the **TLS** rigid-body model (bottom) (Schomaker and Trueblood, 1968). Note that the cutouts occur in the highest quadrant of the ellipsoid. The EAP criteria indicate agreement between all five pairs of thermal ellipsoids. (**b**) A comparison of the observed thermal ellipsoids of the Al5 tetrahedron taken from a refinement of triclinic bikitaite (top) (Bissert and Liebau, 1986) vs. those calculated using the **TLS** rigid-body model (bottom) (Schomaker and Trueblood, 1968). The EAP criteria indicate disagreement in shape and orientation between three pairs of thermal ellipsoids.

TABLE 1. Tetrahedra that pass the EAP criteria (Appendix 2)

Mineral	Reference	Tetrahedron	Libration angle (°)
Microcline	Phillips (1990 personal communication), at 163 K, $C\bar{1}$	Si2o	4.4
		Si2m	4.6
Microcline	Phillips (1990 personal communication), $C\bar{1}$	Al1O	5.3
		Si1m	5.9
		Si2o	5.7
Microcline	Blasi et al. (1984), sample 7813B, $C\bar{1}$	Si1M	5.7
		Si2O	5.7
Microcline	Blasi et al. (1987), $C\bar{1}$	Si2O	5.5
Low albite	Smith et al. (1986), at 13 K, $C\bar{1}$	Al1O	2.8
		Si1M	3.5
Low albite	Harlow and Brown (1980), neutron, $C\bar{1}$	Al1O	5.0
		Si1M	6.3
		Si2M	5.7
Low albite	Harlow and Brown (1980), X-ray, $C\bar{1}$	Al1O	5.1
Low albite	Armbruster et al. (1990), $C\bar{1}$	Al1O	5.0
		Si2O	5.3
Low cordierite	Armbruster (1986a), from Haddam, 100 K, *Cccm*	$T_1$6	3.2
Low cordierite	Armbruster (1986a), from Haddam, *Cccm*	Al11	3.0
		$T_1$6	4.0
Low cordierite	Armbruster (1986b), from Kemiö, *Cccm*	$T_1$6	3.9
		$T_2$3	5.7
Low cordierite	Armbruster (1986b), from Ferry, *Cccm*	Al11	3.1
		$T_1$6	4.5
Low cordierite	Armbruster (1986b), from Sponda, *Cccm*	$T_1$6	4.1
Low cordierite	Cohen et al. (1977), neutron, *Cccm*	$Si_1$6	3.1
Low cordierite	Cohen et al. (1977), X-ray, *Cccm*	$Si_1$6	4.0
Cristobalite	Peacor (1973), at 28 °C, $P4_12_12$	Si	7.0
Coesite	Levien and Prewitt (1981), *C*2/*c*	Si1	4.9
		Si2	4.8
Coesite	Kirfel and Will (1984), *C*2/*c*	Si2	4.9
Coesite	Geisinger et al. (1987), IAM refinement, *C*2/*c*	Si1	4.9
		Si2	4.8
Coesite	Geisinger et al. (1987), IAM+ refinement, *C*2/*c*	Si1	5.0
		Si2	4.9
Coesite	Smyth et al. (1987), at 292 K, *C*2/*c*	Si1	4.9
		Si2	4.8
Coesite	Gibbs et al. (1977), *C*2/*c*	Si1	4.9
Quartz	Young and Post (1962), $P3_212$	Si	5.6
Quartz	Le Page and Donnay (1976), $P3_212$	Si	5.6
Quartz	Levien et al. (1980), $P3_212$	Si	5.4
Quartz	Wright and Lehmann (1981), at 25 °C, $P3_212$	Si	5.5
Quartz	Kihara (1990), at 298 K, $P3_212$	Si	5.7
Natrolite	Artioli et al. (1984), at 20 K, *Fdd*2	Al	2.7
		Si1	3.3
		Si2	3.1
Scolecite	Kvick et al. (1985), at 20 K, *Cc*	Al2	2.6
		Si3	3.0
Scolecite	Joswig et al. (1984), *Fd*	Si2	5.1
		Al1O	4.8
Edingtonite	Kvick and Smith (1983), $C2_12_12$	Al	5.0
		Si1	5.6
Thomsonite	Pluth et al. (1985), *Pncn*	Al1	5.3
		Si1	5.7
		Si2	5.2
		Si3	5.5
Mesolite	Artioli et al. (1986), *Fdd*2	Al1	4.8
		Al2	4.7
		Si3	5.7
Bikitaite	Bissert and Liebau (1986), *P*1	T4	7.1
Anorthite	Kalus (1978), $P\bar{1}$	T2ozi	4.4
Olivine	Miyake et al. (1987), *Pbnm*, Co(03)	Si	3.4
Olivine	Miyake et al. (1987), *Pbnm*, Co(05)	Si	3.1
Olivine	Miyake et al. (1987), *Pbnm*, Co(18)	Si	3.5
Olivine	Miyake et al. (1987), *Pbnm*, Co(20)	Si	3.2
Olivine	Nover and Will (1981), *Pmcn*, Fe(10) P1	Si	3.4
Olivine	Nover and Will (1981), *Pmcn*, Fe(12) P2	Si	3.0
Olivine	Nover and Will (1981), *Pmcn*, Fe(12) P3	Si	3.0
Olivine	Nover and Will (1981), *Pmcn*, Fe(12) P4	Si	3.1
Olivine	Boström (1987), *Pbnm*, Ni = 0.0	Si	3.0
Olivine	Boström (1987), *Pbnm*, Ni = 0.51	Si	2.8
Olivine	Boström (1987), *Pbnm*, Ni = 0.69	Si	2.4
Olivine	Boström (1987), *Pbnm*, Ni = 1.00	Si	3.0
Co-substituted garnet	Ohashi et al. (1981), *Ia3d*	Si	3.2
Zircon	Hazen and Finger (1979), $I4_1/amd$, P = 1 atm	Si	4.2

TABLE 1.—*Continued*

Mineral	Reference	Tetrahedron	Libration angle (°)
Braunite	Moore and Araki (1976), $I4_1/acd$	Si	3.7
Chondrodite	Fujino and Takéuchi (1978), $P2_1/b$	Si	3.0
Andalusite	Winter and Ghose (1979), *Pnnm*, T = 25 °C	Si	3.5
Sillimanite	Winter and Ghose (1979), *Pbmn*, T = 25 °C	Si	3.9
Forsterite	Francis and Ribbe (1980), *Pbnm*, Fo(51)	Si	2.7
Zunyite	Baur and Ohta (1982), $F\bar{4}3m$, Arizona	Si1	6.3
		Al1	2.2
Zunyite	Baur and Ohta (1982), $F\bar{4}3m$, Colorado	Al1	2.2
Helvite	Hassan and Grundy (1985), no. 2, $P\bar{4}3n$	Si	4.2
Rosenhahnite	Wan et al. (1977), $P\bar{1}$	Si3	4.1
Ilvaite	Takéuchi et al. (1983), $P2_1/a$, Tsumo	Si2	3.2
Ilvaite	Finger and Hazen (1987), $P2_1/a$, Seriphos	Si2	3.2
Zoisite	Smith et al. (1987), *Pnma*, 298 K X-ray	Si3	3.0
Kilchoanite	Kimata (1989), *I2cm*	Si1	4.1
Epidote	Gabe et al. (1973), $P2_1/m$, HEP	Si3	3.7
Fluorrichterite	Cameron et al. (1983), Na, $I2/m$, T = 24 °C	T1	4.5
$NaMnSi_2O_6$	Basso et al. (1989), $C2/c$	Si	3.4
Enstatite	Ghose et al. (1986), *Pbca*	Si1	3.3
		Si2	3.0
Jadeite	Cameron et al. (1973), $C2/c$, T = 24 °C	Si	3.5
Acmite	Clark et al. (1969), $C2/c$	Si	3.6
$LiFeSi_2O_6$	Clark et al. (1969), $C2/c$	Si	5.0
Bavenite	Cannillo and Coda (1966), *Cmcm*	Al4	5.2
Feruvite	Grice and Robinson (1989), $R3m$	Si	4.8
Milarite	Sandomirskii et al. (1977), $P6/mcc$	Si	6.8
Searlesite	Ghose and Wan (1976), $P2_1$	Si1	6.0
$K_2Si^{[6]}Si_3{}^{[4]}O_9$	Swanson and Prewitt (1983), T = 25 °C, $P6_3/m$	Si4	4.3
Brannockite	Armbruster and Oberhänsli (1988), $P6/mcc$, no. 1	Si	6.0
Talc	Perdikatsis and Burzlaff (1981), $C\bar{1}$	Si2	4.0
Pyrophyllite	Lee and Guggenheim (1981), $C\bar{1}$	Si1	4.3

temperature (<20 K) libration angle found in framework structures, $\langle\theta\rangle$ = 3.0°. Restricted librational motion of a rigid tetrahedron in olivine may be ascribed to the approximate hexagonal close packing of O atoms in this structure. It is noteworthy that the tetrahedra in coesite, quartz, and cristobalite exhibit increasing $\langle\theta\rangle$ values of 4.9, 5.6, and 7.0°, respectively, at room temperature. This is consistent with the observation that the more open and less dense the framework structure, the greater the librational motion of a TO_4 tetrahedron (Downs and Palmer, 1994).

The mean Δ_{TO} (=0.00040 Å^2) observed for those tetrahedra that are consistent with **TLS** rigid-body motion is very similar to the values $\langle\Delta_{SiO}\rangle$ = 0.0004 Å^2 and $\langle\Delta_{AlO}\rangle$ = 0.0005 Å^2 reported by Kunz and Armbruster (1990) for completely ordered SiO_4 and AlO_4 tetrahedra in low albite. In addition, 97% of the Δ_{TO} data fall within ±0.0015 Å^2, the range suggested by Downs et al. (1990) for rigid Si-O bonds in quartz, cristobalite, and coesite. Because there is no reference atom for a given pair of O atoms, O_1 and O_2, Δ_{OO} is computed as $\Delta_{OO} = |z^2_{O_1O_2} - z^2_{O_2O_1}|$. Note that 99% of the Δ_{OO} values fall within the 0.003 Å^2 limit suggested by Bürgi (1984) for a rigid bond in transition-metal complexes.

IMPLICATIONS OF RIGID-BODY MOTION FOR ADPS

Recently, Downs et al. (1992) found that the isotropic equivalent of the translational motion matrix, $T_{eq}(SiO_4)$, is equal to $B_{eq}(Si)$, suggesting that the ADPs of the central Si atom represent the translational motion of the tetrahedron. Using the EAP method presented here (Appendix 2), a direct comparison is made between the ADPs of the central T atom and the translational motion represented by the **T** matrix determined in the rigid-body analysis. A narrow range of EAP values is found for the 104 tetrahedra that are consistent with **TLS** rigid-body motion, indicating a general agreement between the es-

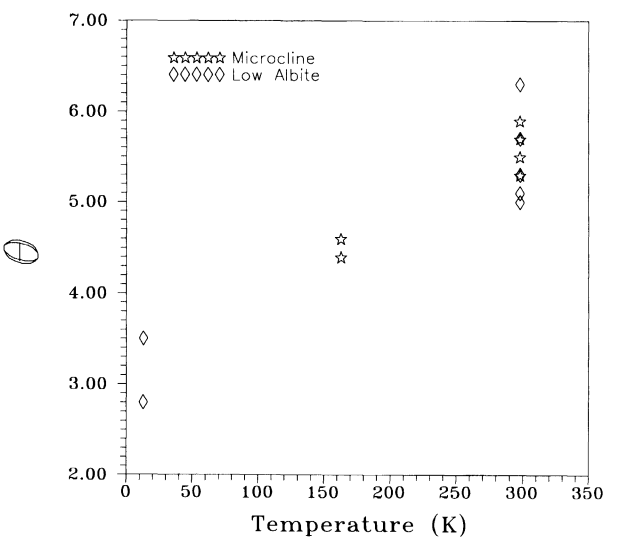

Fig. 2. Libration angle, θ (°), vs. temperature (K) at which the intensity data were collected for the low albite and microcline tetrahedra consistent with **TLS** rigid-body motion (Table 1).

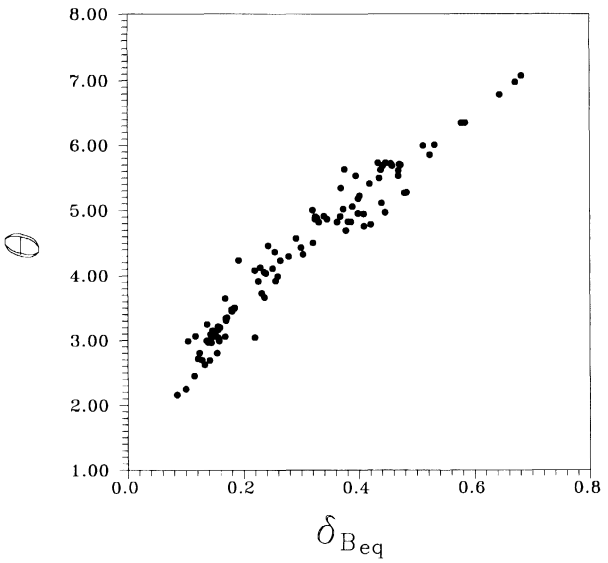

Fig. 3. Libration angle, θ (°), vs. δ_B (Å²), defined as $B_{eq}(O) - B_{eq}(T)$, for the 104 tetrahedra with vibrational motion consistent with **TLS** rigid-body motion. The regression equation computed for these data is $\theta = 1.5 + 11.2\delta_{B_{eq}} - 5.1\delta^2_{B_{eq}}$ ($R^2 = 0.95$).

timated **T** matrix and the ADP matrix for the T atom. However, a much wider range of EAP values is found for the remaining 209 tetrahedra. Consequently, for a TO_4 tetrahedron consistent with **TLS** rigid-body motion, the ADPs of the central T atom represent, in large part, the translational motion of the tetrahedron with little or no librational component.

If the ADPs of the central T atom embody mostly translational motion of a librating rigid tetrahedron, then those of its coordinating O atoms must embody this same translational motion plus additional librational motion. This would suggest that the thermal ellipsoids of O atoms of a TO_4 tetrahedron should be larger than that of the central T atom (Downs et al., 1992). Thus, by subtracting $B_{eq}(T)$ from the average of the four O isotropic equivalent displacement parameters, $B_{eq}(O)$, the difference, $\delta_{B_{eq}}$ [$\delta_{B_{eq}} = B_{eq}(O) - B_{eq}(T)$], should be positively correlated with the librational motion of the tetrahedron as displayed in Figure 3. A regression analysis indicates that 95% of the variation of θ can be explained by a quadratic model containing $\delta^2_{B_{eq}}$. This result supports the observation that the refined thermal ellipsoids of the O atoms are larger than those of the central T atom in a rigid TO_4 tetrahedron, not only because the O atoms are lighter than the T atom, but more importantly because they contain translational and librational motion of the tetrahedron (Downs et al., 1992).

Figure 4a shows considerable scatter in $B_{eq}(T)$ vs. $B_{eq}(O)$ values for the 722 tetrahedra that fail criteria 1 and 2, the EAP criteria, or both (Appendix 2). The wide scatter of $B_{eq}(O)$ values is consistent with that observed by Boisen et al. (1990). For the 104 tetrahedra considered to be consistent with **TLS** rigid-body motion (represented by

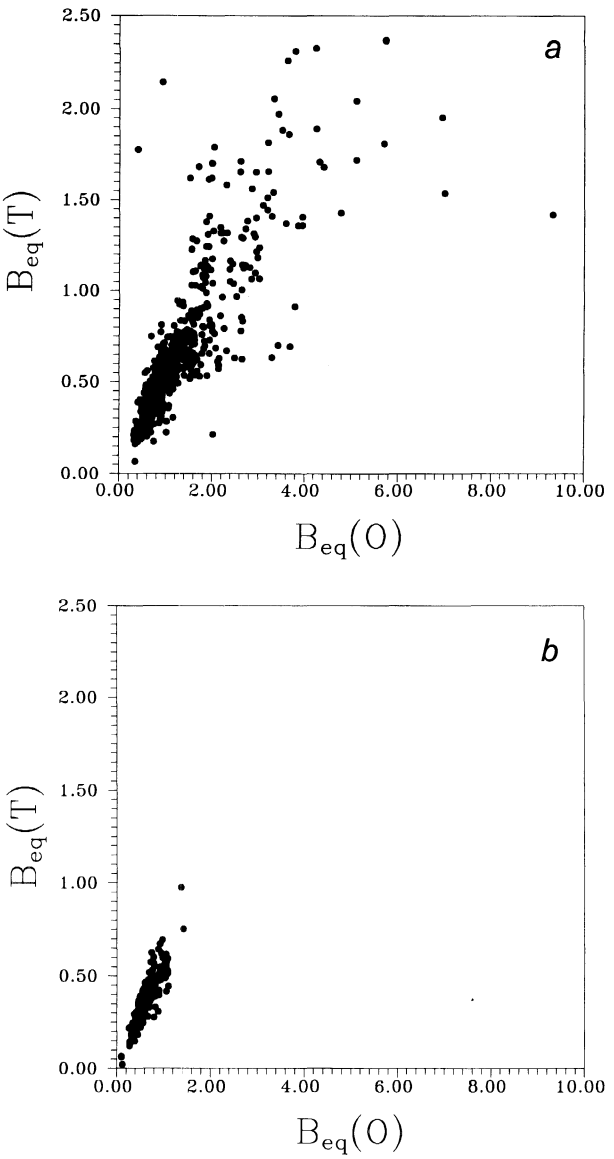

Fig. 4. (**a**) $B_{eq}(T)$ (Å²) vs. $B_{eq}(O)$ (Å²) for tetrahedra that fail rigid T-O bond criteria (1 and 2), EAP criteria, or both (Appendix 2). (**b**) $B_{eq}(T)$ (Å²) vs. $B_{eq}(O)$ (Å²) for tetrahedra that pass all criteria.

dots in Fig. 4b), there is a more limited range of $B_{eq}(T)$ and $B_{eq}(O)$ values. The maximum value of $B_{eq}(O)$ is ~2.0 Å² and is within the range [$B(O) \leq 3.0$ Å²] suggested by Boisen et al. (1990) for $B(O)$ values free of static disorder. The maximum value of $B_{eq}(T)$ consistent with rigid T-O bonds is about 1.0 Å², which may be taken as a limiting value for $B_{eq}(T)$ in structures free of static disorder at standard conditions. A linear regression analysis indicates that $B_{eq}(T)$ is on average one-half of $B_{eq}(O)$, with 74% of the variation in $B_{eq}(T)$ explained in terms of a linear model containing $B_{eq}(O)$.

The coesite data listed in Table 1 constitute most of the room-pressure data set used by Boisen et al. (1990)

in their study of Si-O bond-length variation in coesite. They found that 84% of the variation in d(Si-O) is explained by a linear regression model that includes the parameters, $f_s(O) = 1/[1 - \sec(SiOSi)]$, P, $f_s(Si)$, $B(O)$, and $B(Si)$. Using only the coesite refinement data in which both tetrahedra satisfy the EAP criteria and excluding P as a regressor variable, a step-wise regression involving the remaining four parameters indicates that the best (best in terms of R^2 and mean-square error) regression equation involves only $f_s(O)$ [$d(Si\text{-}O) = 1.75 - 0.313f_s(O)$]. In fact, 90% of the variation in d(Si-O) for the satisfactory coesite data is explained by the parameter $f_s(O)$ alone. Similarly, the best regression for all of the silica polymorph data listed in Table 1 in which all tetrahedra satisfy the EAP criteria also involves only $f_s(O)$ [$d(Si\text{-}O) = 1.75 - 0.304f_s(O)$]. Liebau (1985) asserts that a linear relationship between d(Si-O) and $B(O)$ for the silica polymorphs is obtained when the $B(O)$ data contain static disorder. A test of this assertion indicates there is no linear relationship between d(Si-O) and $B_{eq}(O)$ for the silica polymorphs. This supports our assertion that tetrahedra consistent with rigid-body motion are free of the effects of static disorder.

Acknowledgments

The National Science Foundation is thanked for providing support for this work with grant EAR-8803933. The reviewers are also thanked for suggestions that led to the improvement of this manuscript.

References cited

Armbruster, T. (1986a) Crystal structure refinement and thermal expansion of a Li, Na, Be-cordierite between 100 and 550 K. Zeitschrift für Kristallographie, 174, 205–217.

——— (1986b) Role of Na in the structure of low-cordierite: A single-crystal X-ray study. American Mineralogist, 71, 746–757.

Armbruster, T., and Geiger, C.A. (1993) Andradite crystal chemistry, dynamic X-site disorder and structural strain in silicate garnets. European Journal of Mineralogy, 5, 59–71.

Armbruster, T., and Oberhänsli, R. (1988) Crystal chemistry of double-ring silicates: Structures of sugilite and brannockite. American Mineralogist, 73, 595–600.

Armbruster, T., Bürgi, H.B., Kunz, M., Gnos, E., Brönnimann, S., and Lienert, C. (1990) Variation of displacement parameters in structure refinements of low albite. American Mineralogist, 75, 135–140.

Artioli, G., Smith, J.V., and Kvick, Å. (1984) Neutron diffraction study of natrolite, $Na_2Al_2Si_3O_{10}\cdot 2H_2O$, at 20 K. Acta Crystallographica, C40, 1658–1662.

Artioli, G., Smith, J.V., and Pluth, J.J. (1986) X-ray structure refinement of mesolite. Acta Crystallographica, C42, 937–942.

Basso, R., Lucchetti, G., and Palenzona, A. (1989) Crystallographic and crystal chemical study on a natural $C2/c$ ordered Na-Mn-clinopyroxene from Val di Vara (Northern Apennines, Italy). Neues Jahrbuch für Mineralogie Monatshefte, 59–68.

Baur, W.H., and Ohta, T. (1982) The Si_5O_{16} pentamer in zunyite refined and empirical relations for individual silicon-oxygen bonds. Acta Crystallographica, B38, 390–401.

Bissert, G., and Liebau, F. (1986) The crystal structure of a triclinic bikitaite, $Li[AlSi_2O_6]\cdot H_2O$, with ordered Al/Si distribution. Neues Jahrbuch für Mineralogie Monatshefte, 241–252.

Blasi, A., Brajkovic, A., De Pol Blasi, C., Foord, E.E., Martin, R.F., and Zanazzi, P.F. (1984) Structure refinement and genetic aspects of a microcline overgrowth on amazonite from Pikes Peak batholith, Colorado, U.S.A. Bulletin de Minéralogie, 107, 411–422.

Blasi, A., De Pol Blasi, C., and Zanazzi, P.F. (1987) A re-examination of the pellotsalo microcline: Mineralogical implications and genetic considerations. Canadian Mineralogist, 25, 527–537.

Boisen, M.B., Jr., and Gibbs, G.V. (1990) Mathematical crystallography. In Mineralogical Society of America Reviews in Mineralogy, 15, 406 p.

Boisen, M.B., Jr., Gibbs, G.V., Downs, R.T., and D'Arco, P. (1990) The dependence of the SiO bond length on structural parameters in coesite, the silica polymorphs, and the clathrasils. American Mineralogist, 75, 748–754.

Boström, D. (1987) Single-crystal X-ray diffraction studies of synthetic Ni-Mg olivine solid solutions. American Mineralogist, 72, 965–972.

Boysen, H., Dorner, B., Frey, F., and Grimm, H. (1980) Dynamic structure determination for two interacting modes at the M-point in α- and β-quartz by inelastic neutron scattering. Journal of Physical Chemistry, 13, 6127–6146.

Bürgi, H.B. (1984) Stereochemical lability in crystalline coordination compounds. Transactions of the American Crystallographic Association, 20, 61–71.

Burns, D.M., Ferrier, W.G., and McMullan, J.T. (1967) The rigid-body vibrations of molecules in crystals. Acta Crystallographica, 22, 623–629.

Cameron, M., Sueno, S., Prewitt, C.T., and Papike, J.J. (1973) High-temperature crystal chemistry of acmite, diopside, hedenbergite, jadeite, spodumene, and ureyite. American Mineralogist, 58, 594–618.

Cameron, M., Sueno, S., Papike, J.J., and Prewitt, C.T. (1983) High temperature crystal chemistry of K and Na fluor-richterites. American Mineralogist, 68, 924–943.

Cannillo, E., and Coda, E. (1966) The crystal structure of bavenite. Acta Crystallographica, 20, 301–309.

Chandrasekhar, K., and Bürgi, H.B. (1984) Dynamic processes in crystals examined through difference vibrational parameters ΔU: The low-spin–high-spin transition in tris(dithiocarbamato)iron(III) complexes. Acta Crystallographica, B40, 387–397.

Clark, J.R., Appleman, D.E., and Papike, J.J. (1969) Crystal-chemical characterization of clinopyroxenes based on eight new structure refinements. Mineralogical Society of America Special Paper, 2, 31–50.

Cohen, J.P., Ross, F.K., and Gibbs, G.V. (1977) An X-ray and neutron diffraction study of hydrous low cordierite. American Mineralogist, 62, 67–78.

Destro, R., Pilati, T., and Simonetta, M. (1977) The structure and electron density of *sym*-dibenzo-1,5-cyclooctadiene-3,7-diyne by X-ray analysis of three different temperatures. Acta Crystallographica, B33, 447–456.

Downs, R.T., and Palmer, D.C. (1994) The pressure behavior of α cristobalite. American Mineralogist, 79, 9–14.

Downs, R.T., Gibbs, G.V., and Boisen, M.B., Jr. (1990) A study of the mean-square displacement amplitudes of Si, Al, and O atoms in framework structures: Evidence for rigid bonds, order, twinning, and stacking faults. American Mineralogist, 75, 1253–1267.

Downs, R.T., Gibbs, G.V., Bartelmehs, K.L., and Boisen, M.B., Jr. (1992) Variations of bond lengths and volumes of silicate tetrahedra with temperature. American Mineralogist, 77, 751–757.

Dunitz, J.D., Schomaker, V., and Trueblood, K.N. (1988) Interpretation of atomic displacement parameters from diffraction studies of crystals. Journal of Physical Chemistry, 92, 856–867.

Finger, L.W., and Hazen, R.M. (1987) Crystal structure of monoclinic ilvaite and the nature of the monoclinic-orthorhombic transition at high pressure. Zeitschrift für Kristallographie, 179, 415–430.

Francis, C.A., and Ribbe, P.H. (1980) The forsterite-tephroite series: I. Crystal structure refinements. American Mineralogist, 65, 1263–1269.

Fujino, K., and Takéuchi, Y. (1978) Crystal chemistry of titanian chondrodite and titanian clinohumite of high-pressure origin. American Mineralogist, 63, 535–543.

Gabe, E.J., Portheine, J.C., and Whitlow, S.H. (1973) A reinvestigation of the epidote structure: Confirmation of the iron location. American Mineralogist, 58, 218–223.

Geisinger, K.L., Spackman, M.A., and Gibbs, G.V. (1987) Exploration of structure, electron density distribution and bonding in coesite with Fourier and pseudoatom refinement methods using single-crystal X-ray diffraction data. Journal of Physical Chemistry, 91, 3237–3244.

Ghose, S., and Wan, C. (1976) Structural chemistry of borosilicates, part II: Searlesite, $NaBSi_2O_5(OH)$: Absolute configuration, hydrogen loca-

tions, and refinement of the structure. American Mineralogist, 61, 123–129.

Ghose, S., Schomaker, V., and McMullan, R.K. (1986) Enstatite, $Mg_2Si_2O_6$: A neutron diffraction refinement of the crystal structure and a rigid-body analysis of the thermal vibration. Zeitschrift für Kristallographie, 176, 159–175.

Gibbs, G.V. (1982) Molecules as models for bonding in silicates. American Mineralogist, 67, 421–450.

Gibbs, G.V., Prewitt, C.T., and Baldwin, K.J. (1977) A study of the structural chemistry of coesite. Zeitschrift für Kristallographie, 145, 108–123.

Grice, J.D., and Robinson, G.W. (1989) Feruvite, a new member of the tourmaline group, and its crystal structure. Canadian Mineralogist, 27, 199–203.

Grimm, H., and Dorner, B. (1975) On the mechanism of the α-β phase transformation of quartz. Journal of the Physical Chemistry of Solids, 36, 407–413.

Harlow, G.E., and Brown, G.E., Jr. (1980) Low albite: An X-ray and neutron diffraction study. American Mineralogist, 65, 986–995.

Hassan, I., and Grundy, H.D. (1985) The crystal structures of helvite group minerals, $(Mn,Fe,Zn)_8(Be_6Si_6O_{24})S_2$. American Mineralogist, 70, 186–192.

Hazen, R.M., and Finger, L.W. (1979) Crystal structure and compressibility of zircon at high pressure. American Mineralogist, 64, 196–201.

Hirshfeld, F.L. (1976) Can X-ray data distinguish bonding effects from vibrational smearing? Acta Crystallographica, A32, 239–244.

Hummel, W., Raselli, A., and Bürgi, H.B. (1990) Analysis of atomic displacement parameters and molecular motion in crystals. Acta Crystallographica, B46, 683–692.

Johnson, C.K. (1970) The effect of thermal motion on interatomic distances and angles. In F.R. Ahmed, Ed., Crystallographic computing, p. 207–219. Munksgaard, Copenhagen.

Joswig, W., Bartl, H., and Fuess, H. (1984) Structure refinement of scolecite by neutron diffraction. Zeitschrift für Kristallographie, 166, 219–223.

Kalus, C. (1978) Neue Strukturbestimmung des Anorthits unter Berücksichtigung möglicher Alternativen, Ph.D. dissertation, Ludwig-Maximilians-Universität zu München, Munich, Germany.

Kihara, K. (1990) An X-ray study of the temperature dependence of the quartz structure. European Journal of Mineralogy, 2, 63–77.

Kimata, M. (1989) The crystal structure of mangonaan kilochoanite, $Ca_{2.33}Mn_{0.67}Si_2O_7$: A site-preference rule for the substitution of Mn for Ca. Mineralogical Magazine, 53, 625–631.

Kirfel, A., and Will, G. (1984) Ending the "$P2_1/a$ coesite" discussion. Zeitschrift für Kristallographie, 167, 287–291.

Kunz, M., and Armbruster, T. (1988) Static positional disorder studied by difference vibrational parameters: Na, K-feldspars with variable degree of Si/Al ordering. Zeitschrift für Kristallographie, 182, 166–168.

——— (1990) Difference displacement parameters in alkali feldspars: Effects of (Si,Al) order-disorder. American Mineralogist, 75, 141–149.

Kvick, Å., and Smith, J.V. (1983) A neutron diffraction study of the zeolite edingtonite. Journal of Chemical Physics, 79, 2356–2362.

Kvick, Å., Ståhl, K., and Smith, J.V. (1985) A neutron diffraction study of the bonding of zeolitic water in scolecite at 20 K. Zeitschrift für Kristallographie, 171, 141–154.

Lee, J.H., and Guggenheim, S. (1981) Single crystal X-ray refinement of pyrophyllite-1*Tc*. American Mineralogist, 66, 350–357.

Le Page, Y., and Donnay, G. (1976) Refinement of the crystal structure of low-quartz. Acta Crystallographica, B32, 2456–2459.

Levien, L., and Prewitt, C.T. (1981) High-pressure crystal structure and compressibility of coesite. American Mineralogist, 66, 324–333.

Levien, L., Prewitt, C.T., and Weidner, D.J. (1980) Structure and elastic properties of quartz at pressure. American Mineralogist, 65, 920–930.

Liebau, F. (1985) Structural chemistry of silicates: Structure, bonding, and classification, 347 p. Springer-Verlag, Berlin.

Liebau, F., and Böhm, H. (1982) On the co-existence of structurally different regions in the low-high-quartz and other dilative phase transformations. Acta Crystallographica, A38, 252–256.

Megaw, H.D. (1973) Crystal structures: A working approach, 563 p. Saunders, Philadelphia, Pennsylvania.

Miyake, M., Nakamura, H., Kojima, H., and Marumo, F. (1987) Cation ordering in Co-Mg olivine solid-solution series. American Mineralogist, 72, 594–598.

Moore, P.B., and Araki, T. (1976) Braunite: Its structure and relationship to bixbyite, and some insights on the genealogy of fluorite derivative structures. American Mineralogist, 61, 1226–1240.

Nover, G., and Will, G. (1981) Structure refinements of seven natural olivine crystals and the influence of the oxygen partial pressure on the cation distribution. Zeitschrift für Kristallographie, 155, 27–45.

Ohashi, H., Fujita, T., and Osawa, T. (1981) Structure of $Co_3Al_2Si_3O_{12}$ garnet. Journal of the Japanese Association of Mineralogists, Petrologists, and Economic Geologists, 76, 58–60.

Peacor, D.R. (1973) High-temperature single-crystal study of the cristobalite inversion. Zeitschrift für Kristallographie, 138, 274–298.

Perdikatsis, B., and Burzlaff, H. (1981) Strukturverfeinerung am talk $Mg_3[(OH)_2Si_4O_{10}]$. Zeitschrift für Kristallographie, 156, 177–186.

Pluth, J.J., Smith, J.V., and Kvick, Å. (1985) Neutron diffraction study of the zeolite thomsonite. Zeolites, 5, 74–80.

Rao, K.R., Chaplot, S.L., Choudhury, N., Ghose, S., Hasings, J.M., Corliss, L.M., and Price, D.L. (1988) Lattice dynamics and inelastic neutron scattering from forsterite, Mg_2SiO_4: Phonon dispersion relation, density of states and specific heat. Physics and Chemistry of Minerals, 16, 83–97.

Sandomirskii, P.A., Simonov, M.A., and Belov, N.V. (1977) Crystal structure of synthetic Mn-milarite $K_2Mn_5(Si_{12}O_{30})\cdot H_2O$. Soviet Physics Doklady, 22, 181–183.

Schomaker, V., and Trueblood, K.N. (1968) On the rigid-body motion of molecules in crystals. Acta Crystallographica, B24, 63–76.

Smith, J.V., Artioli, G., and Kvick, Å. (1986) Low albite, $NaAlSi_3O_8$: Neutron diffraction study of crystal structure at 13 K. American Mineralogist, 71, 727–733.

Smith, J.V., Pluth, J.J., Richardson, J.W., and Kvick, Å. (1987) Neutron diffraction study of zoisite at 15 K and X-ray study at room temperature. Zeitschrift für Kristallographie, 179, 305–321.

Smyth, J.R., Smith, J.V., Artioli, G., and Kvick, Å. (1987) Crystal structure of coesite, a high-pressure form of SiO_2, at 15 and 298 K from single-crystal neutron and X-ray diffraction data: Test of bonding models. Journal of Physical Chemistry, 91, 988–992.

Stixrude, L., and Bukowinski, M.S.T. (1988) Simple covalent potential models of tetrahedral SiO_2: Applications to α-quartz and coesite at pressure. Physics and Chemistry of Minerals, 16, 199–206.

Swanson, D.K., and Prewitt, C.T. (1983) The crystal structure of $K_2Si^{VI}Si_3^{IV}O_9$. American Mineralogist, 68, 581–585.

Takéuchi, Y., Haga, N., and Bunno, M. (1983) X-ray study on polymorphism of ilvaite, $HCaFe_2^{2+}Fe^{3+}O_2[Si_2O_7]$. Zeitschrift für Kristallographie, 163, 267–283.

Trueblood, K.N. (1978) Analysis of molecular motion with allowance for intramolecular torsion. Acta Crystallographica, A34, 950–954.

Wan, C., Ghose, S., and Gibbs, G.V. (1977) Rosenhahnite, $Ca_3Si_3O_8(OH)_2$: Crystal structure and the stereochemical configuration of the hydroxylated trisilicate group, $[Si_3O_8(OH)_2]$. American Mineralogist, 62, 503–512.

Winter, J.K., and Ghose, S. (1979) Thermal expansion and high-temperature crystal chemistry of the Al_2SiO_5 polymorphs. American Mineralogist, 64, 573–586.

Wright, A.F., and Lehmann, M.S. (1981) The structure of quartz at 25 and 590 °C determined by neutron diffraction. Journal of Solid State Chemistry, 36, 371–380.

Young, R.A., and Post, B. (1962) Electron density and thermal effects in alpha quartz. Acta Crystallographica, 15, 337–346.

Manuscript received May 2, 1994
Manuscript accepted April 7, 1995

Appendix 1. Data set used

In an examination of criteria 1 and 2, an extensive data set of nonframework silicates was obtained from the literature. The

data were provided by refinements completed on data recorded at room pressure and at or below room temperature, with refined ADPs being reported for all atoms (except H). A structure was accepted for study if reported bond lengths and angles and isotropic equivalent displacement factors could be reproduced and if the ADP matrix for each of its atoms was found to be positive definite. Of the 248 nonframework structures, 231 were accepted, including 94 orthosilicates, 33 sorosilicates, 51 chain silicates, 29 ring silicates, and 41 sheet silicates. This resulted in 357 individual nonframework TO_4, with 99 occurring in orthosilicates, 62 in sorosilicates, 85 in chain silicates, 33 in ring silicates, and 78 in sheet silicates.

Of the 826 TO_4 groups examined in this study, 352 satisfy criteria 1 and 2. These include 166 of the 469 (35%) groups taken from frameworks, 67 of the 99 (68%) from orthosilicates, 42 of the 62 (68%) from sorosilicates, 51 of the 85 (60%) from chain silicates, 17 of the 33 (50%) from ring silicates, and 9 of the 78 (12%) taken from sheet silicates. The observation that nearly one-half (43%) of all the data fail both criteria agrees with similar failure rates observed for a number of molecular compounds (Trueblood, 1978).

Appendix 2. Ellipsoid agreement parameters (EAPs)

Let $\mathbf{M}$ and $\mathbf{M}'$ represent two 3 × 3 real, symmetric, positive definite matrices written with respect to a Cartesian basis, $C = \{\mathbf{i}, \mathbf{j}, \mathbf{k}\}$. Therefore, the graph of the function $[\mathbf{v}]_C^t\mathbf{M}[\mathbf{v}]_C = 1$ represents an ellipsoid in C, where $[\mathbf{v}]_C$ is the triple representative of any vector in C (for notation, see Boisen and Gibbs, 1990). A graph of the function $[\mathbf{v}]_C^t\mathbf{M}'[\mathbf{v}]_C = 1$ represents a different ellipsoid in C if $\mathbf{M} \neq \mathbf{M}'$. The ellipsoid agreement parameters (EAPs) were constructed to provide a measure of the relative physical differences in size, shape, and orientation between two ellipsoids centered at the same position and are based on a strategy devised by Burns et al. (1967).

The first parameter, EAP1, measures the relative agreement between the sizes of two ellipsoids. A reasonable measure of the size of an ellipsoid is provided by the average of its three principal axis lengths. This average is considered as the radius of a sphere that forms an isotropic equivalent of the ellipsoid. For example, the isotropic equivalent of the ellipsoid represented by $\mathbf{M}$, $\mathbf{M}_{eq}$, is computed as $\mathbf{M}_{eq} = \text{trace}(\mathbf{M})/3.0$. EAP1, which measures the relative difference in size between two ellipsoids, is computed as

$$\text{EAP1} = \frac{|\mathbf{M}_{eq} - \mathbf{M}'_{eq}|}{\mathbf{M}_{eq}}.$$

The next parameter, EAP3, measures the difference in orientation between two ellipsoids. Let $\mathbf{U}_\mathbf{M}$ and $\mathbf{U}_{\mathbf{M}'}$ represent unitary matrices consisting of the normalized eigenvectors of $\mathbf{M}$ and $\mathbf{M}'$, respectively, so that

$$\mathbf{U}_\mathbf{M} = [[\mathbf{e}_1]_C \quad [\mathbf{e}_2]_C \quad [\mathbf{e}_3]_C]$$

and

$$\mathbf{U}_{\mathbf{M}'} = [[\mathbf{e}'_1]_C \quad [\mathbf{e}'_2]_C \quad [\mathbf{e}'_3]_C].$$

Note that the normalized eigenvectors of $\mathbf{M}$ and $\mathbf{M}'$ each represent an orthogonal basis, $E = \{\mathbf{e}_1, \mathbf{e}_2, \mathbf{e}_3\}$ and $E' = \{\mathbf{e}'_1, \mathbf{e}'_2, \mathbf{e}'_3\}$, respectively, with a common origin. Therefore, we can consider $\mathbf{U}_\mathbf{M}$ and $\mathbf{U}_{\mathbf{M}'}$ as transformation matrices, such that $\mathbf{U}_\mathbf{M}[\mathbf{v}]_E = [\mathbf{v}]_C$ and $\mathbf{U}_{\mathbf{M}'}[\mathbf{v}]_{E'} = [\mathbf{v}]_C$. Equating these transformations results in

$$\begin{aligned}[\mathbf{v}]_E &= \mathbf{U}_\mathbf{M}^{-1}\mathbf{U}_{\mathbf{M}'}[\mathbf{v}]_{E'} \\ &= \mathbf{U}_\mathbf{M}^t\mathbf{U}_{\mathbf{M}'}[\mathbf{v}]_{E'} \\ &= \mathbf{R}[\mathbf{v}]_{E'}\end{aligned}$$

where $\mathbf{R} = \mathbf{U}_\mathbf{M}^t\mathbf{U}_{\mathbf{M}'}$. Because $\mathbf{R}$ is the product of two unitary matrices, $\mathbf{R}$ is also a unitary matrix and may be considered as a rotation matrix. Because $\mathbf{R}$ represents the angular orientation between E and E', the turn angle of $\mathbf{R}$ provides a measure of the relative difference in orientation between the two ellipsoids represented by $\mathbf{M}$ and $\mathbf{M}'$ (Burns et al., 1967). The turn angle of $\mathbf{R}$, ρ, is found by setting the trace of $\mathbf{R}$ equal to $1 \pm 2\cos\rho$ and represents the amount of rotation about the vector $[\mathbf{l}]_C$ required to bring the basis E' into coincidence with the basis E. Note that because $\mathbf{R}$ is computed from normalized eigenvectors of $\mathbf{M}$ and $\mathbf{M}'$, ρ is dependent on the order in which they are listed by columns in $\mathbf{U}_\mathbf{M}$ and $\mathbf{U}_{\mathbf{M}'}$, respectively. Also note that if, for example, $[\mathbf{e}_1]_C$ is a normalized eigenvector of $\mathbf{M}$, then by symmetry $-[\mathbf{e}_1]_C$ is also a normalized eigenvector of $\mathbf{M}$. Thus, ρ is also dependent on the directions of the eigenvectors listed in $\mathbf{U}_\mathbf{M}$ and $\mathbf{U}_{\mathbf{M}'}$. Systematically permuting the directions and order of the eigenvectors in $\mathbf{U}_\mathbf{M}$ and $\mathbf{U}_{\mathbf{M}'}$, respectively, results in 42 distinct $\mathbf{R}$ matrices and thus 42 distinct ρ values each computed according to $\rho = \cos^{-1}\{[\text{trace}(\mathbf{R}) - 1]/2\}$. The smallest ρ was chosen as the parameter EAP3, thus providing a measure of the difference in orientation between two ellipsoids. If the two ellipsoids each contain a circular cross section, EAP3 is computed as the angle between the eigenvectors perpendicular to the circular section. Finally, if the two ellipsoids are spherical, then EAP3 is zero.

The final parameter, EAP2, measures the relative difference in shape between the two coincident ellipsoids (Burns et al., 1967). A measure of an ellipsoid's shape can be constructed by forming a unit vector from the eigenvalues of the ellipsoid. If we define $S = (\mathbf{s}_1, \mathbf{s}_2, \mathbf{s}_3)$ as the orthonormal shape basis, then

$$\mathbf{s} = \frac{1}{(\lambda_1^2 + \lambda_2^2 + \lambda_3^2)}(\lambda_1\mathbf{s}_1 + \lambda_2\mathbf{s}_2 + \lambda_3\mathbf{s}_3)$$

and

$$\mathbf{s}' = \frac{1}{(\lambda_1'^2 + \lambda_2'^2 + \lambda_3'^2)}(\lambda_1'\mathbf{s}_1 + \lambda_2'\mathbf{s}_2 + \lambda_3'\mathbf{s}_3)$$

where $\mathbf{s}$ and $\mathbf{s}'$ are the shape vectors and $(\lambda_1, \lambda_2, \lambda_3)$ and $(\lambda'_1, \lambda'_2, \lambda'_3)$ are the eigenvalues for $\mathbf{M}$ and $\mathbf{M}'$, respectively. If X is defined as the distance between the endpoints of $\mathbf{s}$ and $\mathbf{s}'$, then according to the law of cosines $X^2 = |\mathbf{s}|^2 + |\mathbf{s}'|^2 - 2(\mathbf{s}\cdot\mathbf{s}') = 2(1 - \mathbf{s}\cdot\mathbf{s}')$. In accordance with Burns et al. (1967), the shape parameter EAP2 is computed as EAP2 = (10000 × X^2). Note that the coefficients of $\mathbf{s}$, λ_1, λ_2, and λ_3, represent the ordered (smallest to largest) triad of eigenvalues of $\mathbf{M}$. The coefficients of $\mathbf{s}'$, λ'_1, λ'_2, and λ'_3, correspond to the (1,1), (2,2), and (3,3) elements of $\mathbf{\Lambda}'$, respectively, where $\mathbf{\Lambda}'$ is computed according to $\mathbf{\Lambda}' = \mathbf{U}_{\mathbf{M}'}^t\mathbf{M}'\mathbf{U}_{\mathbf{M}'} = \mathbf{R}^t\mathbf{U}_\mathbf{M}^t\mathbf{M}'\mathbf{U}_\mathbf{M}\mathbf{R}$ where $\mathbf{R}$ is the rotation matrix used to compute EAP3. For calculated ADPs to be in satisfactory agreement with those observed, the three EAPs must simultaneously satisfy the criteria (A) EAP1 ≤ 0.1, (B) EAP2 ≤ 150, and (C) EAP3 ≤ 20°. A cutoff of ≤0.1 was chosen for criterion (A) because it conforms with the results obtained by the Burns et al. (1967) analysis of size.

As an example, consider the ADP matrix for the Al5 atom from the refinement of triclinic bikitaite (Bissert and Liebau, 1986). Transformed into a Cartesian basis, the ADP matrix becomes

$$\mathbf{M} = \begin{bmatrix} 0.00529 & -0.00048 & -0.00020 \\ -0.00048 & 0.00529 & 0.00012 \\ -0.00020 & 0.00012 & 0.00585 \end{bmatrix}.$$

From a **TLS** analysis of the Al5 tetrahedron, the calculated ADP matrix is

$$\mathbf{M}' = \begin{bmatrix} 0.00553 & -0.00019 & -0.00102 \\ -0.00019 & 0.00583 & 0.00007 \\ -0.00102 & 0.00007 & 0.00594 \end{bmatrix}.$$

The eigenvector matrices and eigenvalues of **M** and **M**′ are

$$\mathbf{U_M} = \begin{bmatrix} 0.71816 & -0.50491 & -0.47886 \\ 0.69343 & 0.57695 & 0.43161 \\ 0.05836 & -0.64202 & 0.76446 \end{bmatrix}$$

$$\lambda_1 = 0.00480, \quad \lambda_2 = 0.00558, \quad \lambda_3 = 0.00604$$

and

$$\mathbf{U_{M'}} = \begin{bmatrix} 0.77592 & 0.04548 & -0.62920 \\ 0.08634 & 0.98036 & 0.17734 \\ 0.62490 & -0.19192 & 0.75675 \end{bmatrix}$$

$$\lambda_1' = 0.00581, \quad \lambda_2' = 0.00469, \quad \lambda_3' = 0.00681$$

respectively.

Using the diagonal elements of both matrices, **M** and **M**′, EAP1 is computed as

$$\text{EAP1} = \frac{|[(0.00529 + 0.00529 + 0.00585)/3] - [(0.00553 + 0.00583 + 0.00594)/3]|}{[(0.00529 + 0.00529 + 0.00585)/3]}$$

$$= |0.00548 - 0.00577|/0.00548$$

$$= 0.053.$$

By systematically permuting the columns of $\mathbf{U_M}$ and $\mathbf{U_{M'}}$, one possible choice of **R** is

$$\mathbf{R} = -1 \times (\mathbf{U_M'U_{M'}}) = \begin{bmatrix} 0.70127 & 0.65357 & -0.28473 \\ -0.66587 & 0.74315 & 0.06585 \\ 0.25463 & 0.14342 & 0.95634 \end{bmatrix}$$

where $(\mathbf{U_M'U_{M'}})$ is multiplied by -1 because it represents an improper rotation. Because this choice of **R** results in the minimum value for ρ, EAP3 = 45.54239°.

Finally, we formulate **s** and **s**′ where $\mathbf{s} = 0.50429\mathbf{s}_1 + 0.58620\mathbf{s}_2 + 0.63408\mathbf{s}_3$ and $\mathbf{s}' = 0.57472\mathbf{s}_1 + 0.46436\mathbf{s}_2 + 0.67384\mathbf{s}_3$. We then compute the distance between the endpoints as $X^2 = 2(1 - \mathbf{s}\cdot\mathbf{s}') = 2(1 - 0.98931) = 0.021380$, which results in EAP2 = 213.80. According to the EAP criteria (A–C) stated above, we conclude that the two ellipsoids are different. Even though EAP1 calculated for **M** and **M**′ indicates the ellipsoids are similar in size, the values of EAP2 and EAP3 indicate large differences in their shape and orientation, respectively. These differences are verified visually by inspection of the observed and calculated thermal ellipsoids drawn for the Al5 atom in Figure 1b.